

Measurement of positron production efficiency from a tungsten monocrystalline target using 4- and 8-GeV electrons

T. Suwada,* S. Anami, R. Chehab,† A. Enomoto, K. Furukawa, K. Kakihara, T. Kamitani, Y. Ogawa, S. Ohsawa, and T. Oogoe

Accelerator Laboratory, High Energy Accelerator Research Organization (KEK), 1-1 Oho, Tsukuba, Ibaraki 305-0801, Japan

H. Okuno

Institute of Particle and Nuclear Studies, High Energy Accelerator Research Organization (KEK), 1-1 Oho, Tsukuba, Ibaraki 305-0801, Japan

T. Fujita, K. Umemori, and K. Yoshida

Hiroshima Synchrotron Radiation Center, Hiroshima University, 2-313 Kagamiyama, Higashi-Hiroshima 739-8526, Japan

R. Hamatsu and K. Sasahara

Department of Physics, Tokyo Metropolitan University, 1-1 Minami-Ohsawa, Hachioji, Tokyo 192-0397, Japan

V. Ababiy, A. P. Potylitsyn, and I. E. Vnukov

Nuclear Physics Institute, Tomsk Polytechnic University, 634050, P.O. Box 25, Tomsk, Russia

(Received 28 May 2001; revised manuscript received 7 November 2002; published 16 January 2003)

Intense positron sources are being widely investigated for the next-generation linear colliders and B factories. A new method utilizing an axially oriented crystal as a positron-production target is one of the bright schemes, since it provides a powerful photon source through channeling and coherent bremsstrahlung processes when high-energy electrons penetrate the target. A series of positron-production experiments with tungsten crystals hit by 4- and 8-GeV single-bunch electron beams were carried out at the KEKB 8-GeV injector linac. Three tungsten crystals with different thicknesses (2.2, 5.3, and 9.0 mm) and those combined with amorphous tungsten plates were tested on a precise goniometer. The positron-production yields were measured with a magnetic spectrometer in the positron momentum (P_{e^+}) range from 5 to 20 MeV/ c . The angle of the $\langle 111 \rangle$ crystal axis with respect to the electron-beam direction was controlled by measuring the relative intensities of the produced positrons as a function of the rotational angle of the goniometer. The results show that the enhancements of the positron yield from crystal targets compared to amorphous targets of the same thickness at $P_{e^+} = 20$ MeV/ c are from 1.5 to 3.7 and from 1.8 to 5.1, depending upon the target thickness for 4- and 8-GeV electrons, respectively.

DOI: 10.1103/PhysRevE.67.016502

PACS number(s): 41.75.Fr, 41.75.Ht, 61.80.Fe, 61.85.+p

I. INTRODUCTION

For future e^+e^- linear colliders and high-luminosity B factories, it is critically important to develop a high-intensity positron source. In a conventional method using an amorphous heavy-metal target, the target thickness is determined to produce mostly low-momentum positrons that can be accepted in the succeeding accelerator section. The momentum acceptance is typically 5–25 MeV/ c , and the optimum thickness is $(4-5)X_0$ (radiation length) for a (4–8)-GeV electron beam. In this case, the only possibility to increase the positron intensity is to increase the incident electron intensity. However, the electron intensity is limited because of a heat load on the target. One promising method utilizing a crystal target was proposed by Chehab *et al.* [1] in 1989. The benefit of this method is its high positron-production effi-

ciency due to channeling radiation (CR) [2] and coherent bremsstrahlung (CB), since CR and CB increase low-energy photons in the radiation process. This results in a thinner target compared with the conventional method. It is expected that the thin target relaxes the problem of the heat load, and that the spatial spread of positrons due to multiple scattering in the target is reduced. Yoshida *et al.* [3] demonstrated a clear enhancement of the positron yield in a tungsten crystal target using a 1.2-GeV electron beam. This new scheme was also tested at the positron station of the KEKB injector linac. The result indicates that, when a hybrid target made of a 1.7-mm-thick tungsten crystal and a 7.0-mm-thick amorphous plate is used and the $\langle 111 \rangle$ crystal axis is oriented along the 3-GeV electron-beam direction, the positron yield is enhanced by 40% compared with that for the disoriented case [4]. Chehab *et al.* also studied the positron yield from the crystal target for (5–40) GeV (mainly 10 GeV) electrons at CERN-SPS [5,6]. Although a positron enhancement is observed, there have so far been only a few experimental results over a wide energy range of a primary electron beam.

On the theoretical side, various simulation studies have

*Electronic address: tsuyoshi.suwada@kek.jp

†Also at LAL, IN2P3-CNRS, Université de Paris–Sud, Bât. 200, B.P. 34, 91898 Orsay, France.

been carried out by various authors. Among them, Baier, Katkov, and Strakhovenko developed a simulation code of the electromagnetic shower formation at the axial alignment of a crystal by using a semi-phenomenological radiation spectrum [7] (also see Artru [8]). This scheme allows one to consider a positron-yield enhancement at the energy range of a few GeV of the initial electrons, which is suitable for the *B* factory injector linac. A substantial enhancement of the positron yield from a crystal target is expected because of the increase in the number of relatively soft photons compared with that from an amorphous target. Thus, more systematic and precise experimental data could help us to understand the complicated mechanism of these elementary radiation processes and to design a high-intensity positron source. A series of experiments [9] to investigate the positron yields using various crystal targets are underway for incident electron energies lower than 8 GeV. In the succeeding sections, we will report on the measurements by 4- and 8 GeV electrons with targets of tungsten crystals and those with amorphous tungsten plates behind them.

II. EXPERIMENTAL SETUP

A. Electron beam

Our experiment was performed at the energy analyzer line in the beam switchyard of the KEKB 8-GeV injector linac [10]. An electron beam with a pulse width of 10 ps (*S*-band single bunch) impinged on a tungsten crystal target at a repetition rate of 25 and 2 Hz with the energy of 4 and 8 GeV, respectively. The beam charge (0.2 nC/bunch) was measured by a wall-current monitor for each pulse. The transverse profile of the electron beam at the target was monitored by a 100- μm -thick fluorescent screen monitor (99.5% Al_2O_3 + 0.5% CrO_3) during the experiment. The transverse beam size was 1–1.5 mm (full width at half maximum, FWHM) in diameter. The angular spreads of the electron beam were measured with a wire scanner to be about 123 (23) and 121 (41) μrad in the horizontal and vertical directions to the beam axis for the 4- (8-) GeV electrons, respectively. While the electron beam impinged on the target after passing through a vacuum window made of 100- μm -thick stainless steel (SUS304), the angular spread of the electron beam at the target was estimated to be 0.2 (0.1) mrad in total at 4 (8) GeV by taking into account multiple scattering. The condition for axial channeling requires that the angle of particle incidence with respect to the crystallographic axis be less than the critical angle ϑ_c [11] defined by

$$\vartheta_c = \sqrt{\frac{2U_0}{E}}, \quad (1)$$

where U_0 is the depth of the potential well in a crystal and E is the electron energy. The critical angle of the axial channeling condition in the tungsten crystal is 0.61 (0.43) mrad at 4 (8) GeV, which is less than the angular spread of the incident electrons.

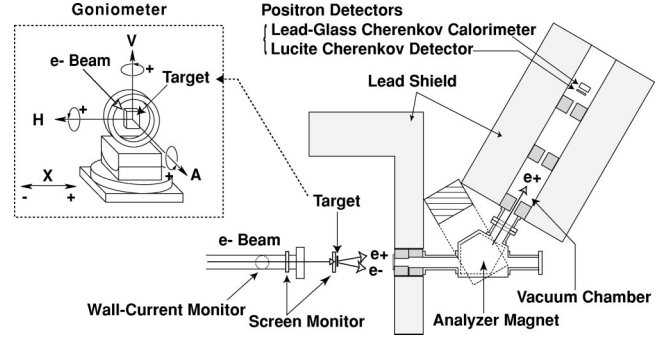


FIG. 1. Schematic drawing of the experimental setup.

B. Tungsten monocrystalline target

Three tungsten monocrystalline targets W_c with different thicknesses (2.2, 5.3, and 9.0 mm) were tested either alone or in combination with an amorphous tungsten plate W_a . The surface mosaic spreads of these crystals on both sides were measured by an *x*-ray scattering method to be 1.5, 0.5, and 0.5 mrad for 2.2-, 5.3-, and 9.0-mm-thick crystals, respectively. W_a 's with different thicknesses from 3 to 18 mm with 3-mm steps were also installed on a horizontal movable stage to the beam axis at 82.5 mm behind the crystal target. They were used for combined targets. Several other W_a 's with thicknesses of up to 28 mm were also mounted on a crystal target holder, which made it possible to calibrate the positron yield.

C. Positron spectrometer

Figure 1 shows a schematic drawing of the experimental setup. This comprises a positron-production target mounted on a precise goniometer and a positron spectrometer. The positrons emitted from the target in the forward direction were momentum analyzed by the magnetic field in a momentum range lower than 20 MeV/*c*, where the deflection angle was 60° from the beam axis. The positron trajectories were determined by five collimators installed before and behind the momentum-analyzer magnet. They were kept in a vacuum at a pressure level of 10^{-1} Pa. An entrance window of the vacuum chamber was made of a 50- μm -thick polyimide film. The momentum-analyzed positrons were detected with a 5-mm-thick transmission-type Lucite Cherenkov detector and a 20-mm-thick total-absorption-type lead-glass calorimeter with photomultiplier tubes. The lead blocks surrounding the detectors suppressed any background caused by electromagnetic showers generated upstream of the beam line by off-momentum electrons, and caused by electromagnetic showers generated at the collimators and at a beam dump behind the positron spectrometer.

The acceptance $\Delta P \Delta \Omega$ of the positron spectrometer was obtained by using the detector simulation code GEANT3 [12] at each positron momentum (see Table I). The typical geometrical and momentum acceptances are about 1 msr and 2.4% ($\Delta P/P$, FWHM) at $P_{e^+} = 20$ MeV/*c*.

D. Data-acquisition system

Since the shortly bunched positrons were emitted, the number of positrons per bunch was measured as a pulse

TABLE I. Acceptance of the positron spectrometer.

P_{e^+} (MeV/c)	Acceptance ($\Delta P \Delta \Omega$) [$10^{-4} \times (\text{MeV}/c) \text{ sr}$]
5	1.08 ± 0.03
10	2.47 ± 0.07
15	3.80 ± 0.10
20	4.81 ± 0.12

charge from each detector. Signals from the positron detectors and the signal of the wall-current monitor were sent to a data-acquisition system using a PC/Linux-based CAMAC analog-to-digital converter, where all signal charges were simultaneously digitized and recorded. The goniometer could rotate the crystal target around two axes (the horizontal H and vertical V axes) by pulse motors. The angular resolutions of the goniometer were 10.5 and 34.9 $\mu\text{rad}/\text{pulse}$ in the H and V axes, respectively. The $\langle 111 \rangle$ crystal axis with respect to the electron beam was determined by changing the relative rotational angles around the two axes with steps of 2 mrad. The positron yields were measured for each target as a function of the rotational angle of the goniometer and as a function of the positron momentum.

III. EXPERIMENTAL RESULTS

A. Measurement and data analysis

Since a wide dynamic range for the positron-yield measurement was required, depending on the target thickness, the positron momentum, and the electron energy E_{e^-} , high voltages (HV's) applied to the photomultipliers were carefully adjusted in order to maintain the good linearity of each signal before each target measurement. After the HV adjustment, the channeling condition along the $\langle 111 \rangle$ crystal axis at which the positron yield was maximum was controlled by measuring the positron yield as a function of the V and H angles of the goniometer. A rocking curve was measured as a function of the goniometer rotational angle around the H axis, while the angle around the V axis was fixed at the angular position giving the peak yield. Twenty beam-pulse measurements were performed at the same H angle with steps of 2 mrad. The data corrections were made for pedestals in positron charge measurements, for backgrounds, and for the electron-beam intensity. The beam-associated background data were also measured under the condition with the magnetic field off and with the target away. The background data were carefully analyzed and subtracted from the raw data. The data measured by a lead-glass calorimeter (total energy of positrons) and a Lucite Cherenkov detector (number of positrons) were consistent with each other within the experimental uncertainty.

B. Rocking curves

The results of rocking-curve measurements for the W_c 's at $P_{e^+} = 20 \text{ MeV}/c$ are shown in Figs. 2, where the relative positron yields are plotted as a function of the goniometer rotational angle. Figures 2(a)–2(c) and Figs. 2(d)–2(f) show

the results for $E_{e^-} = 4$ and 8 GeV together with the simulation curves, respectively. The experimental results clearly indicate that the peak width of the rocking curve is much larger than the critical angle of the channeling electrons. The peak width becomes broader as the crystal target is thicker. This variation is shown in Fig. 3, where the peak width is shown as a function of the target thickness at $P_{e^+} = 20 \text{ MeV}/c$ for $E_{e^-} = 4$ and 8 GeV. Here, the peak width was obtained by a least-squares fitting to data points with a Lorentzian function. This figure indicates a strong dependence of the peak width on the target thickness. The growth of the peak width with the increase of the crystal thickness was also obtained in our previous experiment [13] for thin tungsten crystals less than $0.63X_0$ in the 1 GeV energy region.

The simulations for the rocking curves are done by using the simple model [14], in which the coherent bremsstrahlung process in the crystal target is considered as a main contributor to the primary radiation process and the following electromagnetic processes are approximated by the EGS4 simulation code [15] in amorphous tungsten. These simulation results reproduced the rocking curves measured for the thin tungsten crystals in the 1 GeV energy region within the difference of 15%. However, when we apply this code to the thicker target at the higher-energy region, the agreement is not very good, as shown in Figs. 2. Although the simulation results give the measured enhancement of the positron yield, the peak width of the rocking curve is smaller compared to the measured value, especially for the thicker target. These results show that our present simulation code is too simple to describe the development of electromagnetic shower processes in thick crystals. We presume that two physical processes need to be taken into account in the simulation code. One is the contribution to the positron production from the axial channeling radiation and radiation from the secondary particles. Another is coherent electron and, especially, positron scattering (doughnut scattering effect) near the crystallographic axis [16,17]. In the simulation code, the multiple scattering of the charged particles in a crystal is treated similarly as in amorphous matter. This approximation is widely used in similar simulation codes [7,8,20,21]. The doughnut scattering effect, which results in the turning of the charged particles with respect to their azimuthal angles around the crystallographic axis, leads to the changing of the positron angular distribution when the axis direction does not coincide with the initial electron-beam propagation direction. In a recent experiment [18] with a 1.7-mm-thick tungsten crystal at $E_{e^-} = 500 \text{ MeV}$, the influence of this effect was observed for the $\langle 111 \rangle$ axis misalignment angles greater than 200 mrad (about five to seven times of the root-mean-squared angle of electron multiple scattering in this crystal). These processes could have an influence on the rocking-curve peak width, and more sophisticated simulation code is under development. From the view point of a practical application of crystalline targets, the broad peak characteristics of the rocking curve will relax the accuracy for target alignment.

C. Enhancement of the positron yield

An enhancement of the relative positron yield was obtained from the rocking curves. Here, the enhancement is

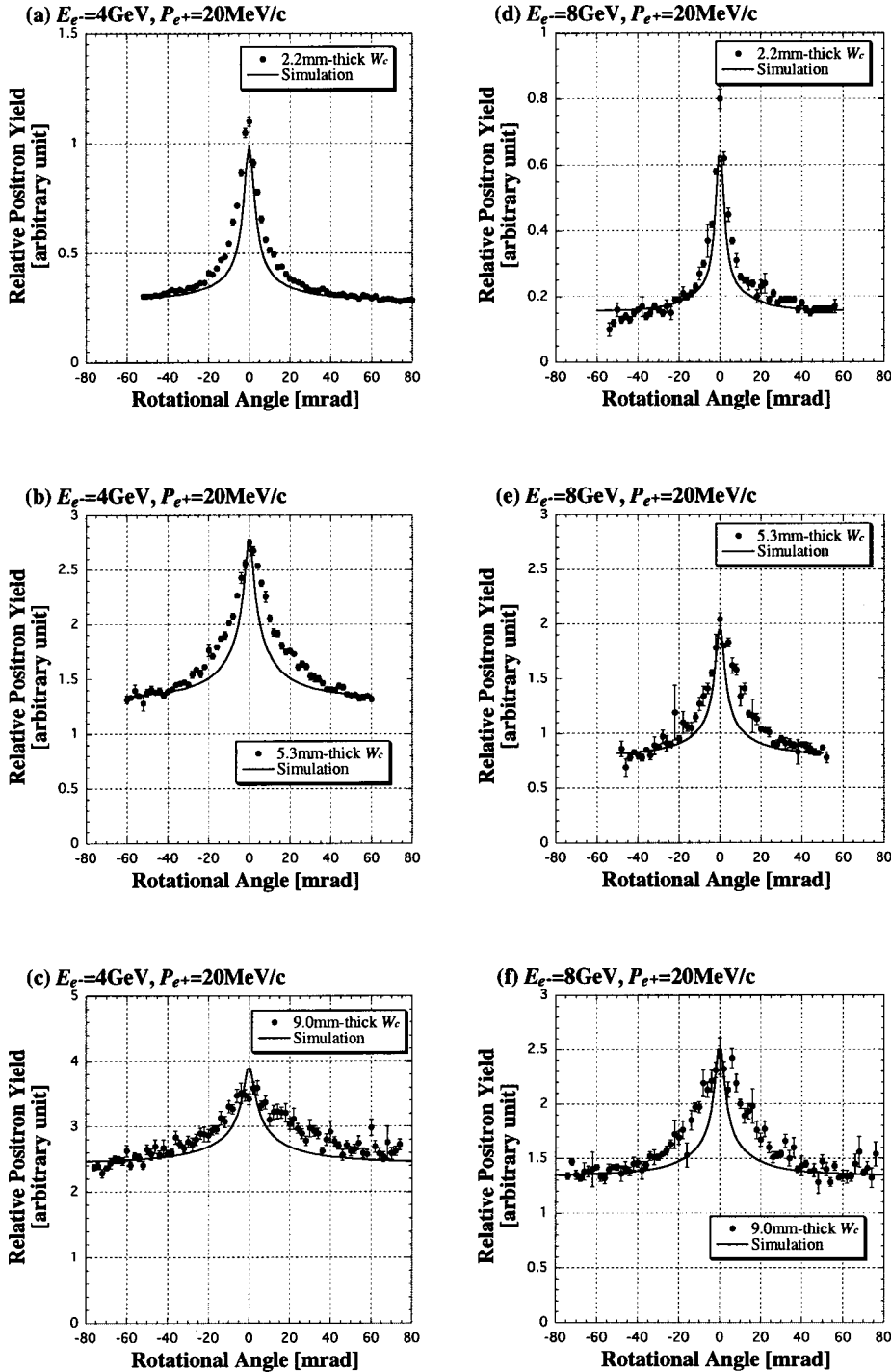


FIG. 2. Rocking curves measured at $P_{e^+} = 20 \text{ MeV}/c$ for (a) 2.2-mm-thick W_c , (b) 5.3-mm-thick W_c , and (c) 9.0-mm-thick W_c at $E_e = 4 \text{ GeV}$, and for (d) 2.2-mm-thick W_c , (e) 5.3-mm-thick W_c , and (f) 9.0-mm-thick W_c at $E_e = 8 \text{ GeV}$ as a function of the goniometer rotational angle around the H axis. It is noted that the different high voltages were applied to the positron detectors for the measurements at $E_e = 4$ and 8 GeV in order to maintain the good linearity of the detector signals. The solid curves through the data are based on the simulation. The curves are normalized by using the data at the off-axis region.

defined by the ratio of the peak yield (on-axis) to the yield at the base region (off-axis) 50 mrad apart from the crystal axis in the H scan. The observed enhancements at $P_{e^+} = 20 \text{ MeV}/c$ for both of the W_c 's and the combined targets as a function of the target thickness are shown in Figs. 4. Here, the total thickness of the target was used for the combined targets. The result shows that the enhancement factor decreases with an increase of the total target thickness, and beyond 14 mm at $E_e = 4 \text{ GeV}$, the crystal works to decrease the positron yields more than the amorphous (disoriented) targets. This could be explained by the fact that the

effective radiation length for crystal targets is decreased appreciably by channeling radiation and coherent bremsstrahlung effects. Since the photons generated by channeling and coherent bremsstrahlung processes are relatively softer than those produced in bremsstrahlung, they produce correspondingly soft e^+e^- pairs that are sensitive to multiple scattering in the amorphous converter. Thus, with a given collimation, these soft e^+e^- pairs have larger angles and are less easily accepted than e^+e^- pairs produced in amorphous targets.

The momentum dependence of the enhancement for the crystal targets was also measured in the momentum range of

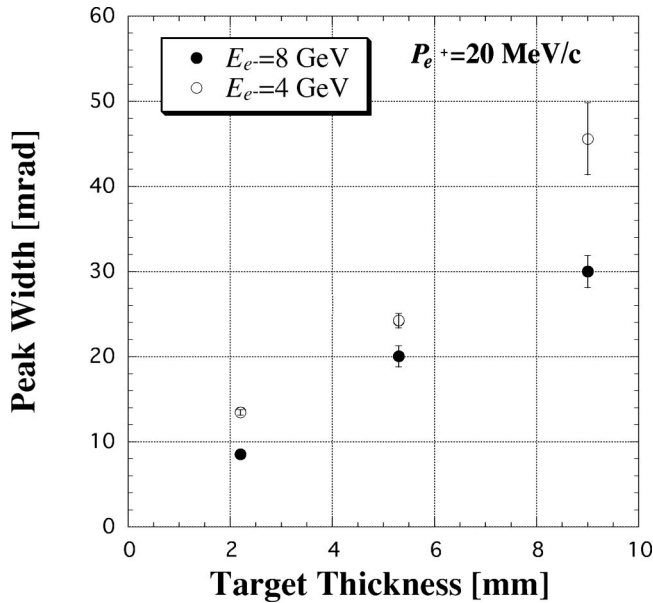


FIG. 3. Variations in the peak width of the rocking curve at $P_{e^+}=20$ MeV/c for $E_{e^-}=4$ and 8 GeV as a function of the target thickness.

5–20 MeV/c (see Table II). The result shows that the momentum dependence of the enhancement is not very strong in the present measurement. Also shown in the table are the results of a simulation by Baier and Strakhovenko [19] at $E_{e^-}=8$ GeV, which reproduce the data on the enhancement and its momentum dependence well within the experimental accuracy.

The incident electron-energy dependence of the positron-yield enhancement at $P_{e^+}=20$ MeV/c for the 2.2-mm-thick W_c is shown in Fig. 5. Here, the previous experimental result [13] measured at $E_{e^-}=1.0$ GeV is also shown in the figure. The result shows that the enhancement increases monotonically with the increase of the incident electron energy, and is consistent with the simulation calculations [13,19].

D. Positron-production efficiency

The absolute values of the measured positron yields were calibrated by using the data for the W_a targets. The positron-production efficiencies for the different W_a target thicknesses were calculated by using the GEANT3 code in which the whole geometry of the experimental setup was taken into account. Here, the positron-production efficiency is defined as the ratio of the number of detected positrons to the number of incident electrons. Figures 6(a) and 6(b) show the variations of the positron-production efficiency as a function of the total target thickness for $P_{e^+}=20$ MeV/c at $E_{e^-}=4$ and 8 GeV, respectively. The results of the calculations are shown in thick solid curves. The experimental data points (shown in open diamonds) for the W_a targets were normalized to the calculations at the thickness of 9.0 mm. The calculations reproduce well the experimental data points over the wide range of the W_a target thicknesses. The positron-production efficiencies for different thicknesses of the crystal and combined targets were obtained by multiplying the en-

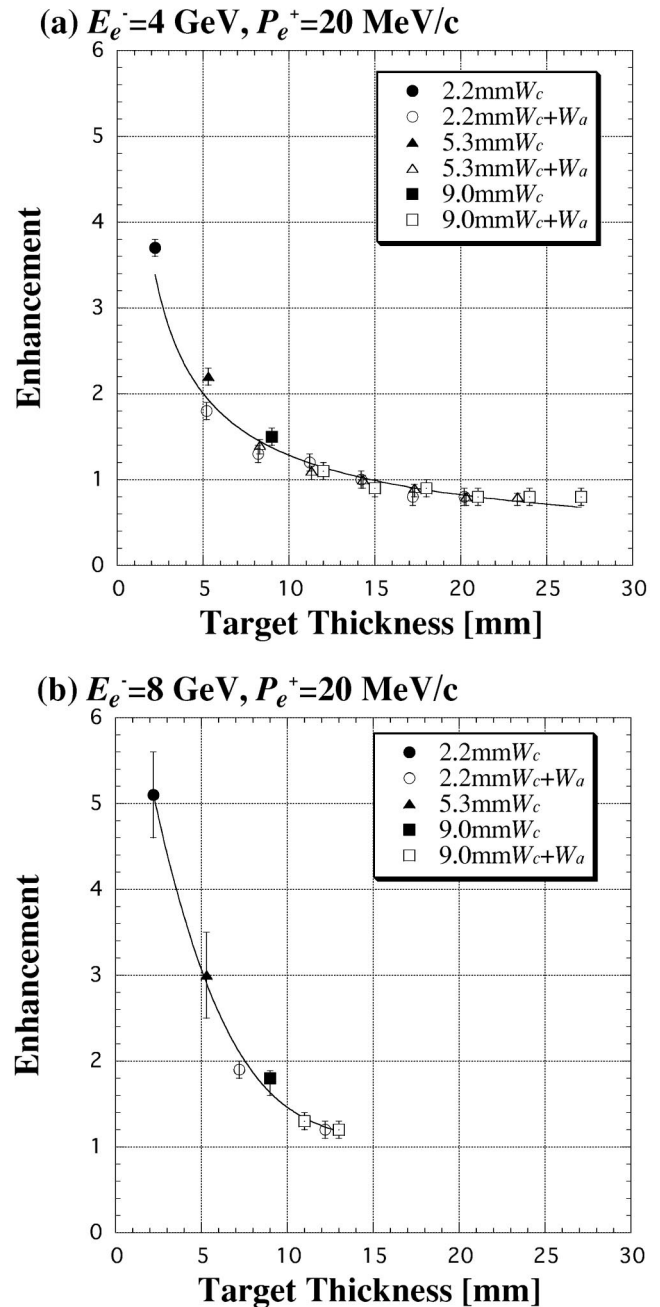


FIG. 4. Variations in the enhancement of the positron yield at $P_{e^+}=20$ MeV/c for (a) $E_{e^-}=4$ GeV and (b) $E_{e^-}=8$ GeV as a function of the target thickness. The solid curves drawn through the data are only to guide the eye.

hancements to the experimental data of the W_a targets and plotted in the figures. The obtained results clearly show that the absolute positron yield for the 9.0-mm-thick W_c was enhanced by 26% with $P_{e^+}=20$ MeV/c at $E_{e^-}=4$ and 8 GeV, compared with the maximum positron yield obtained for the amorphous targets. The result also shows that for each combined-target data at $E_{e^-}=4$ GeV, the target thickness giving the peak point at which the maximum positron yield is obtained is reduced in comparison with that of the amorphous target. This means that the effective radiation length

TABLE II. Momentum dependence of the positron-yield enhancement for the crystal targets. The values given in parentheses are the simulation results by Baier and Strakhovenko [19].

P_{e^+} (MeV/c)	$E_{e^-} = 4$ GeV			$E_{e^-} = 8$ GeV		
	2.2-mm W_c	5.3-mm W_c	9.0-mm W_c	2.2-mm W_c	5.3-mm W_c	9.0-mm W_c
5	3.3 ± 0.1	2.2 ± 0.1	1.5 ± 0.2	5.0 ± 1.5	2.9 ± 0.5	2.1 ± 0.3
10	3.6 ± 0.3	2.3 ± 0.1	1.5 ± 0.2	6.5 ± 0.6 (6.0 ± 0.5)	3.4 ± 0.7 (3.2 ± 0.3)	2.3 ± 0.4 (2.1 ± 0.2)
15	3.5 ± 0.1	2.2 ± 0.1	1.7 ± 0.3	6.2 ± 0.8 (5.5 ± 0.3)	3.2 ± 0.5 (3.2 ± 0.2)	2.0 ± 0.2 (2.0 ± 0.1)
20	3.7 ± 0.1	2.2 ± 0.1	1.5 ± 0.1	5.1 ± 0.5 (5.4 ± 0.2)	3.0 ± 0.5 (2.9 ± 0.1)	1.8 ± 0.2 (1.8 ± 0.1)

for the aligned crystal target becomes shorter than that in an amorphous target. It is understood that the reduction of the radiation length and little momentum dependence on the thickness of the crystal part are clearly caused by the crystal effect due to the photon conversion of the incident electron.

E. Discussions

Our experimental results agree well with those by Chehab *et al.* [20], who used 6- and 10-GeV electron beams at CERN-SPS, although the positron momentum acceptances of the two experiments are different. In our experiment, the momentum range is $5 \leq P_{e^+} \leq 20$ MeV/c and the angular acceptance is limited to $0 \leq \theta \leq 10$ mrad, but in the experiment of Chehab *et al.*, $5 \leq P_{e^+} \leq 45$ MeV/c and $0 \leq \theta \leq 440$ mrad. In the positron source of the future linear colliders [21], the momentum range of the positrons to be accelerated is typically designed as $5 \leq P_{e^+} \leq 25$ MeV/c, P_{\perp}

≤ 10 MeV/c in order to collect positrons as much as possible with a dedicated matching optical system. In our experimental conditions, although the momentum range coincides with that of the accelerator positron source, the angular acceptance is much smaller, because the dynamic range of the positron detectors mainly limits it. But the positron enhancement does not change so much depending on the positron emission angle [3]. This is because the distribution of positron emission angles is determined predominantly by multiple scattering for a thick target.

It should be mentioned that the present measurement was made with a shortly-bunched (10-ps) electron beam and with the intensity of 0.2 nC/bunch. On the other hand, the measurement by Chehab *et al.* was made with a high-duty tertiary electron beam from CERN-SPS. The agreement between both measurements indicates that the crystal preserves its lattice structure under the impact of the high-instantaneous-intensity electron beam, where the electron beam may cause a specific kind of crystal lattice excitation rather than simple heating. This is very encouraging for the application of the crystal target to a positron source of the future linear collider, where a very shortly bunched beam will be used.

Here, we give some discussions and considerations in the application of the tungsten crystal target to a realistic high-intensity positron source. There are two items to be seriously studied; (1) the heat-load problem and (2) the radiation damage problem for a crystal target. As for the heating problem, the temperature rise affects the field level of the atomic potential in the crystal target and, thus, it mitigates the channeling effect. The radiation damage of the crystal also reduces the crystal effect and leads to the reduction of positron yield. These effects have been studied theoretically and experimentally by some authors [21–23]. Baier and Strakhovenko [22] estimated the energy deposition in a tungsten crystal based on their theory of electromagnetic processes on which all the known coherent radiation processes were taken into account. They calculated the deposited energy depending upon the target thickness when electrons with the energy range of 10–300 GeV impinge the target with an axial alignment. Their result shows that at $E_{e^-} = 10$ GeV the energy deposition in the crystal is about half compared to that for the maximal amorphous yield accompanied by the same positron yield. This result shows that the heating of a tungsten

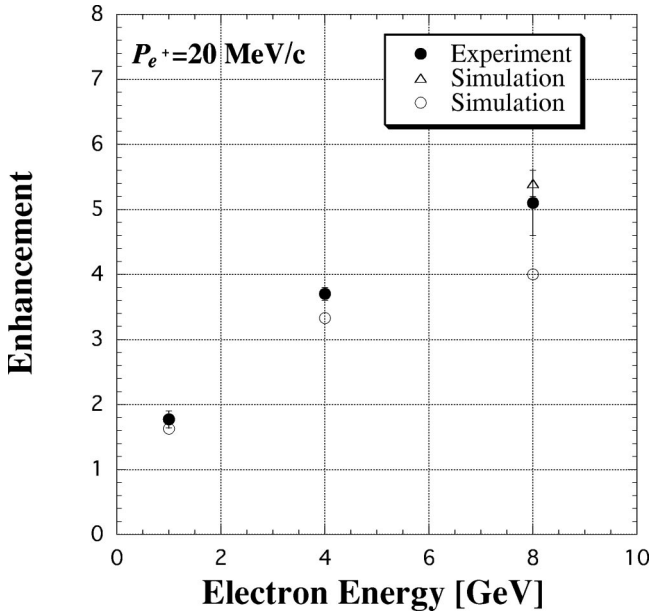


FIG. 5. Incident electron-energy dependence of the positron-yield enhancement at $P_{e^+} = 20$ MeV/c for the 2.2-mm-thick tungsten monocrystalline target. The open circles and triangle show the simulation result by our code [see the text (Sec. III B) for details] and by Baier and Strakhovenko [19], respectively.

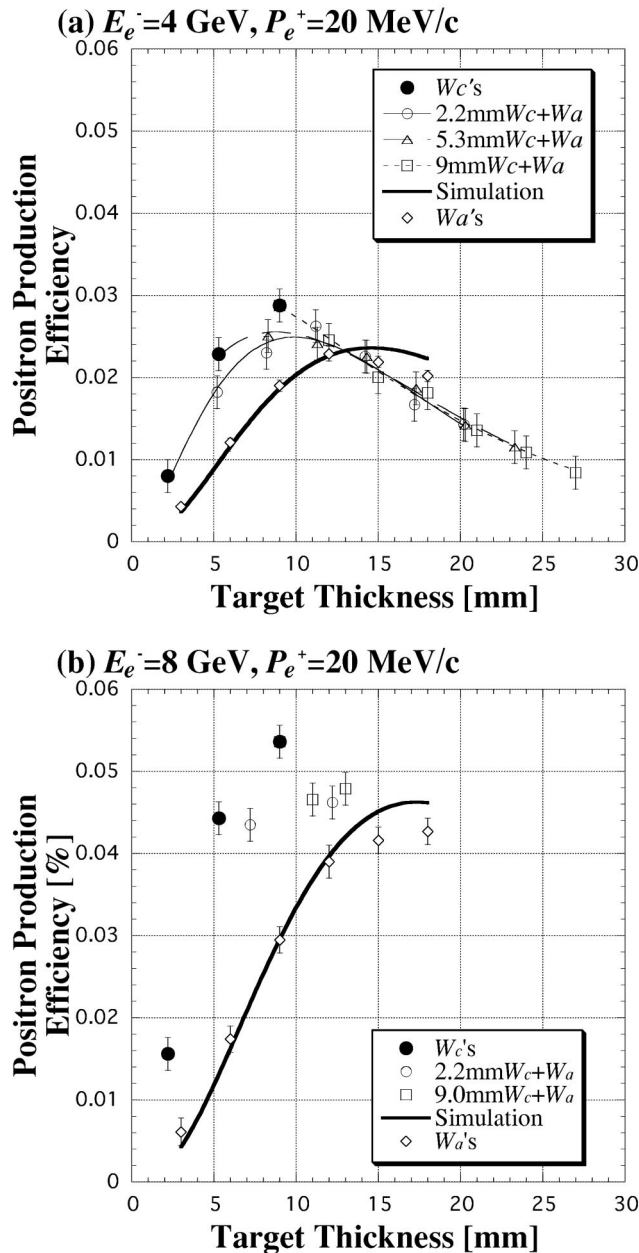


FIG. 6. Positron production efficiencies measured for the crystal and combined targets at $P_{e^+} = 20 \text{ MeV}/c$ for (a) $E_e^- = 4 \text{ GeV}$ and (b) $E_e^- = 8 \text{ GeV}$. The thick solid curves drawn through the data obtained for the W_a 's are based on a simulation. The other thin curves drawn through the data are only to guide the eyes.

crystal can be appreciably reduced due to the lower level of the deposited energy.

Artru *et al.* [21] also estimated the temperature rise in a tungsten crystal designed for the linear-collider positron source. Their result shows that, when the crystal–amorphous plate combined target (4-mm-thick W_c + 4-mm-thick W_a) is used, the deposited energy in the crystal is about 1/4 of that in the 8-mm-thick amorphous tungsten, and the temperature

rise is at an allowable level ($\leq 600^\circ$) without so much degradation of the positron yield.

As for the radiation damage effect, Artru *et al.* [23] tested on a 0.3-mm-thick tungsten monocrystal exposed in front of the positron converter of the SLAC Linear Collider (SLC) up to the integrated electron flux of $2 \times 10^{18} e^-/\text{mm}^2$, which corresponds to about 100 h for the nominal linear-collider operation. No damage on the mosaic spread of the crystal was found after the irradiation. Although these estimations and observations are encouraging, further studies are highly desirable for the practical application.

IV. SUMMARY

Positron-production experiments by 4- and 8-GeV electrons hitting an axially oriented tungsten monocrystalline target were successfully carried out at the KEKB injector linac. The positron-production efficiencies from the crystal targets were measured as a function of the target thickness and as a function of the positron momentum. The results show that when the $\langle 111 \rangle$ crystal axis was aligned along the incident electron-beam direction, a large positron-yield enhancement was observed for thin crystalline targets. The enhancement factor decreases as the target thickness increases. The positron-yield enhancement by a crystalline target is almost constant in the momentum range of 5–20 MeV/c , and for the 2.2-mm-thick crystalline target it increases monotonically with the increase of the incident electron energy in the range of 1–8 GeV. It is interesting to note that at $E_e^- = 8 \text{ GeV}$, the positron yield from the 9.0-mm-thick crystal target is larger than the maximum yield attainable from the amorphous target with the optimum thickness (18 mm). In addition, even for a combined target with a 2.2-mm-thick crystal and a 5.0-mm-thick amorphous tungsten plate, we can get almost the same amount of positron yield comparable to that from the amorphous target for maximum yield. The maximum positron yield for the 9-mm-thick crystal target was larger by 26% than the largest yield given by the 14-mm-thick amorphous target at $E_e^- = 4 \text{ GeV}$ and that by the 18-mm-thick amorphous target at $E_e^- = 8 \text{ GeV}$. It is of great benefit to apply such a crystal target to a high-intensity positron source required for high-luminosity e^+e^- colliders.

ACKNOWLEDGMENTS

We would like to thank the operators of the KEKB injector linac for their help during this experiment. The tungsten crystals were fabricated under a joint effort by the Institute of Physical-Technical Problems, Ministry of Atomic Energy of RF, Dubna, Russia and the Institute of Solid-State Physics, Russian Academy of Sciences, Chernogolovska, Russia. This work was supported by the collaborative R&D program at High Energy Accelerator Research Organization (KEK), and partially supported by the Russian Ministry of Education, Regional Programs, Grant No. 1478.

- [1] R. Chehab, F. Couchot, A. R. Nyaiesh, F. Richard, and X. Artru, Proceeding of the 1989 IEEE Particle Accelerator Conference (PAC'89), Chicago, IL (unpublished), p. 283.
- [2] A.H. Sørensen and E. Uggerhøj, *Sci. Am.* **260** (6), 70 (1989).
- [3] K. Yoshida *et al.*, *Phys. Rev. Lett.* **80**, 1437 (1998).
- [4] M. Inoue *et al.*, *Nucl. Instrum. Methods Phys. Res. B* **173**, 104 (2000).
- [5] R. Chehab *et al.*, Proceedings of the XVIII International LINAC Conference (LINAC2000), Monterey, CA, 2000 (unpublished), p. 143.
- [6] R. Chehab *et al.*, in *Proceedings the Vth International Symposium on Radiation from Relativistic Electrons in Periodic Structures (RREPS'01), Lake Aya, Altai Mountains, Russia, 2001*, edited by Yu.L. Pivovarov [*Nucl. Instrum. Methods Phys. Res. B* (to be published)].
- [7] V.N. Baier, V.N. Katkov, and V.M. Strakhovenko, *Nucl. Instrum. Methods Phys. Res. B* **103**, 147 (1995).
- [8] X. Artru, *Nucl. Instrum. Methods Phys. Res. B* **48**, 278 (1990).
- [9] H. Okuno *et al.*, in *Proceedings the Vth International Symposium on Radiation from Relativistic Electrons in Periodic Structures (RREPS'01), Lake Aya, Altai Mountains, Russia, 2001*, (Ref. [6]).
- [10] I. Sato *et al.*, KEK Report No. 95-18 1996 (unpublished) (in Japanese).
- [11] J. Lindhard, K. Dan. Vidensk. Selsk. Mat. Fys. Medd. **34**, 1 (1965).
- [12] CERN Program Library Long Writeup W5013, CERN, Geneva, 1994.
- [13] S. Anami *et al.*, *Nucl. Instrum. Methods Phys. Res. B* **183**, 459 (2001).
- [14] B.N. Kalinin *et al.*, *Nucl. Instrum. Methods Phys. Res. B* **145**, 209 (1998).
- [15] W. R. Nelson, H. Hirayama, and D. W. O. Rogers, SLAC Report No. 265, 1985 (unpublished).
- [16] J.A. Golovchenko, *Phys. Rev. B* **13**, 4672 (1976).
- [17] A.I. Akhiezer and N.F. Shul'ga, *High Energy Electrodynamics in Matter* (Gordon and Breach, Luxemburg, 1996).
- [18] E. Bogomazova *et al.*, *Proceedings of the Vth International Symposium on Radiation from Relativistic Electrons in Periodic Structures (RREPS'01), Lake Aya, Altai Mountains, Russia, 2001* (Ref. [6]).
- [19] V.N. Baier and V.M. Strakhovenko, e-print hep-ph/0203058.
- [20] R. Chehab *et al.*, *Phys. Lett. B* **525**, 41 (2002).
- [21] X. Artru *et al.*, *Part. Accel.* **59**, 19 (1998).
- [22] V.N. Baier and V.M. Strakhovenko, *Nucl. Instrum. Methods Phys. Res. B* **155**, 403 (1999).
- [23] X. Artru *et al.*, Report No. LAL-RT-98-02, 1998 (unpublished).